

Line shape considerations in ultrafast 2D NMR

Boaz Shapira, Adonis Lupulescu, Yoav Shrot, and Lucio Frydman*

Department of Chemical Physics, Weizmann Institute of Science, 76100 Rehovot, Israel

Received 10 September 2003

Abstract

We have recently proposed and demonstrated an approach that enables the acquisition of 2D nuclear magnetic resonance (NMR) spectra within a single scan. The approach is based on spatially encoding the spins' evolution along the indirect domain with the aid of a magnetic field gradient, and subsequently decoding this information numerous times over the course of the signal acquisition while spins are subject to a train of gradient echoes. The present paper discusses further considerations pertaining the 2D line shapes arising from this new way of collecting NMR data. Specific issues that are hereby addressed include (i) the effects introduced by fast relaxation onto the spatial encoding process, particularly the line widths and line shapes that will then arise in the frequency domain; (ii) approaches capable of correcting for the mixed-phase kernels resulting in these fast-relaxation cases, corresponding in essence to spatially encoded analogs of the TPPI and hypercomplex time-domain acquisition procedures; (iii) the enveloping characteristics imposed by the use of discrete excitation pulses on the attainable spectral widths along the indirect domain; and (iv) an analysis of the signal-to-noise characteristics of the methodology, with experimental corroborations of theoretical predictions and an illustration of the method's capabilities to analyze protein solutions in the mM-range concentration. © 2003 Elsevier Inc. All rights reserved.

Keywords: Two-dimensional spectroscopy; Ultrafast NMR; Purely absorptive line shapes; Limits of detection; Protein 2D NMR

1. Introduction

Multidimensional spectroscopy plays a central role in all contemporary applications of nuclear magnetic resonance (NMR) [1–3]. 2D NMR in particular has become over the years a basic tool in the elucidation of the chemical, structural, and dynamic characteristic of a wide variety of systems, spanning from simple inorganic and organic molecules, through pharmaceuticals and medicinal compounds, and onto complex biological structures. In spite of the very different systems that are studied and goals sought by 2D NMR experiments in chemical and biochemical analyses, all such pulse sequences share an overall design laid out by Jeener, Ernst and co-workers [4,5] when they first introduced this form of spectroscopy. According to this well-known paradigm

Preparation/Excitation – Evolution(t_1) – Mixing
– Detection(t_2) (1)

frequencies in 2D NMR are monitored as a function of an evolution time t_1 encoding an initial interaction Ω_1 , and of a time t_2 that encodes a final coupling Ω_2 . This final time t_2 incorporates the usual data acquisition process involved in 1D Fourier spectroscopy, leaving the scanning of the initial time domain to a parametric incrementation of t_1 . The t_1 parameter thus becomes a variable time delay, of which numerous independent values are needed for a proper Fourier decoding of the Ω_1 interactions. As each of these t_1 incrementations corresponds in essence to an independent 1D NMR experiment, it follows that even when dealing with systems possessing abundant signal-to-noise ratios (S/N), nD NMR acquisitions will be inherently longer than their 1D counterparts.

We have recently proposed an alternative route to acquiring multidimensional NMR data, that enables the acquisition of complete spectra within a single data acquisition scan [6]. The approach (Fig. 1) is based on

* Corresponding author. Fax: +972-8-9344123.

E-mail address: lucio.frydman@weizmann.ac.il (L. Frydman).

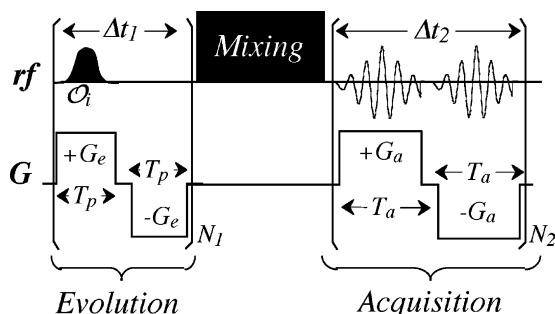


Fig. 1. Generic scheme of ultrafast 2D NMR, based on an initial spatial encoding of the indirect evolution frequencies by a train of N_1 Rf excitation pulses applied at constant frequency offset increments $\Delta O = |O_{i+1} - O_i|$. This creates a spatial winding of the evolving spin coherences, which is then preserved throughout the mixing period and decoded multiple (N_2) times as a function of t_2 with the aid of an oscillating gradient $\pm G_a$.

replacing the serial t_1 incrementation used by 2D spectroscopy for monitoring the Ω_1 evolution, with a parallelized approach whereby these internal frequencies are employed to impart a spatial encoding of the spins' coherences. Such spatial encoding can be carried out in a relatively straightforward manner with the aid of an oscillating magnetic field gradient, applied in synchrony with a series of spatially selective excitation or refocusing pulses. Following a conventional mixing period the spatial encoding imparted in this manner can be inspected repeatedly at equal time delays Δt_2 with the aid of a second oscillating field gradient; when combined with a suitable data acquisition and processing protocol, all this can reveal the nature of both the Ω_1 -driven encoding as well as of the post-mixing Ω_2 internal frequencies. Given the lack of constraints imposed by the gradient-based encoding and decoding procedures the methodology appears to be in principle general, and hence its overall scheme could find applications in several instances where S/N is not the experiment's main time limitation.

Together with the introduction of this new 2D data acquisition approach our recent reports also focused on certain practical aspects of the protocol, including theoretical descriptions of the line shapes arising in the absence of relaxation, spectral width considerations, and the artificial folding of peaks as well as methods for their eventual unfolding [7,8]. In this paper we expand on these previous discussions, and present both theoretical derivations and measurements that further validate and extend them. Particular attention is placed on describing and verifying the excitation details involved in this form of spectroscopy, on the sensitivity limits of the approach within the context of its current implementation, and on an evaluation of the effects that spin relaxation will have on the process of spatial encoding. In this latter case we also introduce and exemplify routes which can account for the mixed-phase line shapes that spin relaxation

during the encoding will produce—in essence the spatial-based analogs of established time-domain procedures such as time-proportional phase incrementation (TPPI) and hypercomplex data acquisition [9,10].

2. Experimental

All spectral results described in this work were measured on a Bruker Avance 800 MHz NMR spectrometer incorporating a multiple-resonance inverse gradient probehead as testing equipment. Although a triple-axis gradient set was available only the longitudinal z -axis, endowed with the strongest field gradients and associated to the longest spatial dimensions, was used for spatially encode the 2D NMR spectra. This gradient's maximum strength ($G_z \approx 62$ G/cm), typical switching times (≈ 10 μ s) and associated sample dimension (1.8 cm) were calibrated prior to the measurements. When dealing with a need for implementing additional homospoil or water-suppression gradient-pulses, we found it beneficial to use some of the remaining (x or y) gradients available in the system. A variety of Matlab 6.5 software programs (The MathWorks) were written for the sake of processing the data, simulating the effects of various pulse sequences and estimating the acquisition conditions. All simple chemicals and solvents were obtained from Aldrich and used as purchased; lyophilized ^{15}N -labeled ubiquitin was purchased in its histidine-tagged form from Asla (Latvia) and used to prepare an aqueous solution following literature guidelines.

3. Results and discussion

3.1. Indirect-domain line shapes and the effects of relaxation

As basis to the following discussion we shall consider the general ultrafast 2D acquisition scheme introduced in Fig. 1, whereby spins in a sample are sequentially excited by a train of N_1 gradient-refocused excitation pulses. Such scenario is akin to the one employed in the discussions presented in [6,7]; as in such studies we shall once again consider that the excited spins end up distributed in packets that are uniformly spaced along the sample's length L at coordinates

$$\left\{ z_j = \frac{L}{N_1 - 1} [j - (N_1 - 1)/2] \right\}_{j=0, N_1-1},$$

and characterized by independent indirect-domain evolution times $t_1(z_j) = C(z_j - z_{N_1})$. The spatio-temporal constant C in this expression defines the extent of time encoding experienced by the excited spin-packets and equals the ratio between the overall t_1 evolution time

and L . Under ideal excitation conditions where the Δt_1 dwell time equals twice the excitation pulse width T_p ,

$$|C| \approx \left| \frac{2T_p(1 - N_1)}{L} \right|.$$

During the course of their respective evolution times t_1 each of the excited spin-packets will accumulate a coherent precession phase $\Omega_1 t_1$, while experiencing a decay $\exp(-t_1/T_2)$. Following the mixing period the signals originated by these various spin-packets are monitored as a function of the wavenumber $k = \gamma_a \int_0^t G_a(t') dt'$ unraveling their respective z positions, as well as of an acquisition time t_2 encoding their direct-domain Ω_2 frequencies. As this latter direct-domain encoding is conventional we do not consider it further, and focus only on the signal's dependence as a function of the k variable. This can then be described as

$$S(k) = \sum_{j=0}^{N_1-1} A_j \exp\{iC\Omega_1(z_j - z_{N_1})\} \times \exp\left\{\frac{-C(z_j - z_{N_1})}{T_2}\right\} \exp\{ikz_j\} \quad (2)$$

The A_j here are coefficients reflecting the amplitudes that for a given chemical site, will characterize the signals arising from a particular spin-packet j . For an uniform sample these amplitude coefficients are constant and equal to M_o/N_1 , M_o being the signal intensity generated by the magnetization associated to a particular site when considered all over the sample.

Eq. (2) is analogous to the Eq. (6) presented in Ref. [7], except for the inclusion of an additional spin-spin relaxation decay over the course of the t_1 evolution. This addition can be accounted for simply by replacing $\tilde{\Omega}_1 = \Omega_1 + i/T_2$; our previous analysis can then be followed to derive a generalized indirect-domain line shape expression that in the $N_1 \gg 1$ limit reads

$$S(k) = \frac{M_o}{N_1} \cdot \exp\{i\tilde{\Omega}_1 T_p(N_1 + 1)\} \cdot \frac{\exp\{i(\tilde{\Omega}_1 T_p N_1 + \frac{kL}{2})\} - \exp\{-i(\tilde{\Omega}_1 T_p N_1 + \frac{kL}{2})\}}{\exp\{i(\tilde{\Omega}_1 T_p + \frac{kL}{2N_1})\} - \exp\{-i(\tilde{\Omega}_1 T_p + \frac{kL}{2N_1})\}} \quad (3)$$

It is instructive to consider the results stemming from this expression for a variety of T_2 values, as spin relaxation will eventually influence the line shapes characterizing peaks along the indirect domain of ultrafast NMR spectroscopy. For the extreme $T_2 \rightarrow \infty$ condition these line shape kernels have already been derived and shown to lead to [7]

$$S(k) = \frac{M_o \exp\{i\Omega_1(N_1 + 1)\}}{N_1} \cdot \frac{\sin(\Omega_1 T_p N_1 + \frac{kL}{2})}{\sin(\Omega_1 T_p + \frac{kL}{2N_1})} \quad (4)$$

In the $\Omega_1 \approx 0$ neighborhood this represents a Sinc-like line shape

$$S(k) \approx \frac{M_o}{N_1} \frac{\sin(\frac{kL}{2})}{\left(\frac{kL}{2N_1}\right)}, \quad (5)$$

flanked by “ghost-peaks” at multiples of $2\pi N_1/L$. We consider next the line effects arising when considering a slow spin-spin relaxation processes ($2T_p N_1 \ll T_2$). All $e^{\pm T_p N_1/T_2}$ exponents in Eq. (3) can then be expanded as $1 \pm (T_p N_1/T_2)$, leading to the approximate line shape expression

$$S(k) = \frac{M_o}{N_1} e^{iT_p(N_1+1)\Omega_1} e^{-T_p(N_1+1)/T_2} \left\{ \frac{\sin(\Omega_1 T_p N_1 + \frac{kL}{2})}{\sin(\Omega_1 T_p + \frac{kL}{2N_1})} \times \left[1 - i \frac{T_p}{T_2} \text{ctg}\left(\Omega_1 T_p + \frac{kL}{2N_1}\right) \right] + i \frac{T_p N_1}{T_2} \frac{\cos(\Omega_1 T_p N_1 + \frac{kL}{2})}{\sin(\Omega_1 T_p + \frac{kL}{2N_1})} \right\} \quad (6)$$

for $\Omega_1 \approx 0$ the resulting kernel will now be given by

$$S(k) = \frac{M_o}{N_1} e^{-T_p(N_1+1)/T_2} \times \left\{ \frac{\sin(\frac{kL}{2})}{\left(\frac{kL}{2N_1}\right)} + i \frac{T_p}{T_2} \left[\frac{N_1 \cos(\frac{kL}{2})}{\frac{kL}{2N_1}} - \frac{\sin(\frac{kL}{2})}{\left(\frac{kL}{2N_1}\right)^2} \right] \right\} \quad (7)$$

The main differences arising upon comparing this equation with the relaxation-free $\Omega_1 = 0$ Sinc function in Eq. (5) involve the appearance of an overall attenuation prefactor, as well as of an imaginary component. The dispersive-like character taken by this imaginary component can be appreciated more clearly on considering the fast $2T_p N_1 \gg T_2$ relaxation limit, whereby the exponential terms $e^{i\tilde{\Omega}_1 T_p N_1}$ in the numerator of Eq. (3) have decayed to zero. The whole line shape function can then be approximated as

$$S(k) = -\frac{M_o}{N_1} \cdot \frac{\exp\{i\tilde{\Omega}_1 T_p\} \exp\{i\frac{kL}{2}\}}{\exp\{i(\tilde{\Omega}_1 T_p + \frac{kL}{2N_1})\} - \exp\{-i(\tilde{\Omega}_1 T_p + \frac{kL}{2N_1})\}} \quad (8)$$

On making the short-dwell-time assumption $T_p/T_2 \ll 1$ one can further expand the denominators as well, to retrieve the line shape function

$$S(k) = \frac{M_o}{N_1} \cdot e^{i\frac{kL}{2}} e^{i\Omega_1 T_p} \cdot \frac{1}{2} \frac{\left(\frac{T_p}{T_2}\right) + i\left(\Omega_1 T_p + \frac{kL}{2N_1}\right)}{\left(\frac{T_p}{T_2}\right)^2 + \left(\Omega_1 T_p + \frac{kL}{2N_1}\right)^2} \quad (9)$$

Aside from the $e^{i\frac{kL}{2}}$ factor, which is an artifact stemming from the fact that the $z = 0$ sample coordinate does not

coincide with its $t_1 = 0$ counterpart, one can recognize in this expression a real Lorentzian component peaking at $k \approx -C\Omega_1$ plus a dispersive imaginary line shape that is also centered at this k value.

Fig. 2 illustrates for the $\Omega_1 = 0$ condition and a variety of T_2/N_1T_p regimes, examples of the line shapes that are predicted by the full expression in Eq. (3), as well as by the analytical approximations in Eqs. (5), (7), and (9). As can be appreciated both numerical as well as analytical descriptions coincide in their prediction of a continuous progression from the purely real Sinc-like line shape expected when $T_2 = \infty$ to the complex *Absorptive* + *i-Dispersive* extreme expected in the $N_1T_p \gg T_2$ limit. The Lorentzian line shapes arising in this limit from the spatial encoding are characterized by a full-width at half-height that is $(4N_1T_p)/(LT_2)$ in k units, or equivalently by $2/T_2$ in the kHz units of the ν_1 -domain. All these theoretical derivations are fully born out by experiments, presented for a similar N_1T_p/T_2 progression in Fig. 3. The right-hand side of this Figure shows real and imaginary components of line shapes observed along the indirect k/ν_1 -axis, in data sets that were acquired using a mixing-less scheme based on the sequence

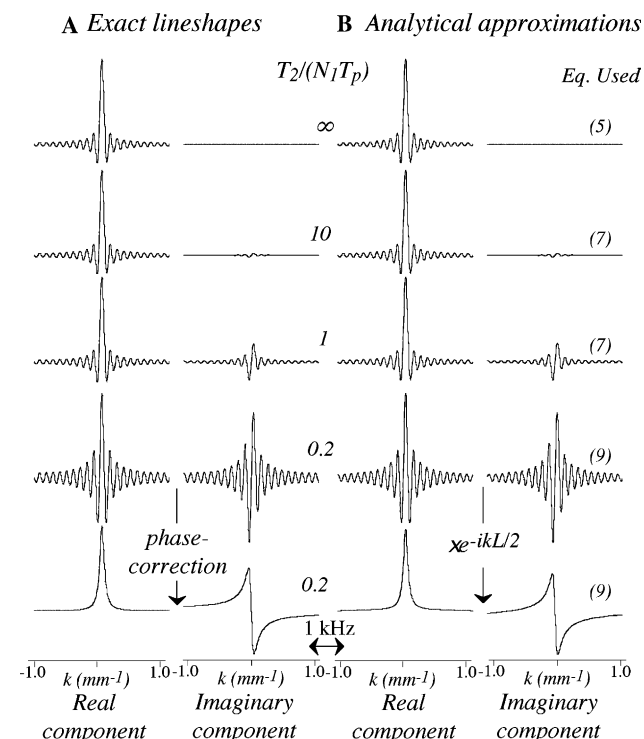


Fig. 2. Changes evidenced by the Real and Imaginary components of the $S(k)$ line shapes introduced in the text, as a function of progressively shorter T_2 relaxation times during the spins' excitation. All kernels were calculated for $\Omega_1 = 0$ assuming $T_p = 0.1$ ms, $N_1 = 50$, and sample length $L = 20$ mm. (A) Numerical predictions arising from Eq. (3). (B) Analytical predictions stemming from Eqs. (5)–(9). Traces in the bottom row were phase-corrected to account for the $\exp(i(kL/2))$ factor in Eq. (9). The double-headed arrow corresponds to the equivalent spanned by a 1 kHz frequency range.

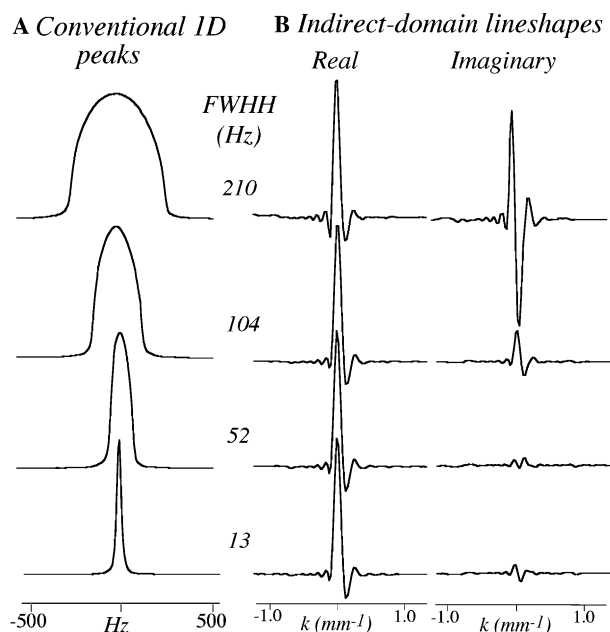


Fig. 3. Experimental corroboration of the $S(k)$ expectations illustrated in Fig. 2, as manifested by the appearance of imaginary line shape components with increasingly faster rates of signal decay. (A) Artificially broadened 1D NMR peaks. (B) Corresponding line shapes arising along the k/ν_1 -domain of single-scan 2D NMR experiments. In these cases mixing-less sequences were applied on-resonance to an HDO signal, using $N_1 = 61$, $\gamma_e G_e = 178$ kHz/cm, $\gamma_a G_a = 69$ kHz/cm, $T_p = 167$ μ s, square excitation pulses.

shown in Fig. 1. As the T_2 of the on-resonance HDO ^1H signal used for these experimental tests was much longer than the acquisition time explored along the indirect t_1 domain, no dispersive components affected the “natural” $S(k)$ line shapes observed under optimized single-scan conditions (Fig. 3, bottom). We envision that under normal acquisition conditions, this situation will be quite common when measurements are made on small molecules. In order to manipulate the apparent relaxation effects in this HDO sample an artificial broadening was thus introduced, by dialing in a series of increasingly stronger field gradients with the aid of the x -axis shim control. The line shape changes that are then observed as a function of effective line broadening depict the predicted emergence of a dispersive imaginary component along ultrafast's NMR indirect domain.

As in conventional 2D NMR, an undesirable aspect of the imaginary components that are introduced by spin relaxation into the $S(k)$ function is the appearance of a phase-twisting in the line shapes describing the full 2D peaks. Indeed the fact that relaxation introduces a dispersive-like imaginary component into the $S(k/\nu_1)$ line shape for $t_2 = 0$, coupled to the usual *Absorptive*(Ω_2) + *i-Dispersive*(Ω_2) line shape that will arise along the direct frequency domain after Fourier transform (FT) versus t_2 , means that dispersive-like additions will characterize the peaks arising in the fully processed

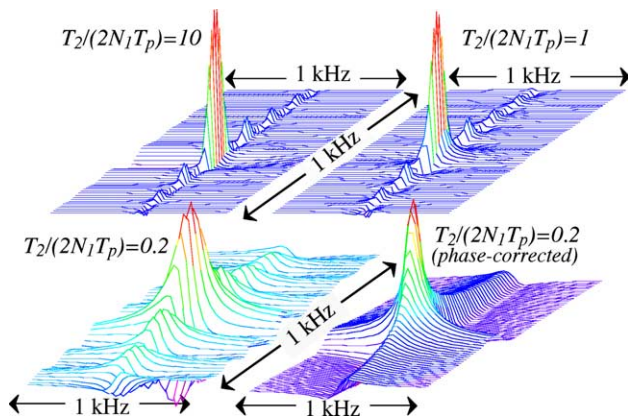


Fig. 4. Changes evidenced by the Real components of 2D $S(k/v_1, v_2)$ line shapes, as a function of progressively shorter T_2 relaxation times. Stack plots were calculated as for Fig. 2A, except for the addition of an additional decay as a function of t_2 . Notice the emergence of the typical mixed-phase line shape for sufficiently short decays, upon accounting for the first-order $\exp(i(kL/2))$ factor (bottom-right plot).

2D NMR spectrum. Fig. 4 illustrates such line shapes for a series of increasingly smaller $T_2/(N_1 T_p)$ ratios.¹ As known from the high-resolution multidimensional NMR literature such mixed-phase character is an artifact worth getting rid of, and numerous approaches have been discussed on how to carry out such artifact suppression. These include the “States-Haberhorn-Ruben” acquisition of quadrature amplitude-modulated data sets, acquisitions of signals arising from echo and anti-echo coherence transfer pathways, and TPPI-based acquisitions of a single nD NMR data set. All such approaches are known to be, in a certain sense, equivalent to one another [12]. Yet the different nature whereby peaks are generated in ultrafast NMR—which is free from the parametric time encoding and subsequent Fourier processing underlying all these equivalent approaches—implies that these phase-incremented schemes will have to be modified in order to eliminate the dispersive k -space components introduced in Fig. 4. The following paragraph analyzes further these differences, and discusses some of the approaches capable of dealing with them.

3.2. Purely absorptive peak shapes in ultrafast 2D NMR

Imaginary components arise in ultrafast experiments due to the presence of spin relaxation during the course of the indirect-domain evolution. Because of the spatial encoding occurring throughout these experiments this decay results in a spatial distortion of the excited spin coherences, whereby amplitudes cease to subtend a

constant $M_0/N_1 z$ profile and acquiring instead an $\exp[-C(z - z_{N_1})/T_2]$ z -dependence. When considering that the acquisition gradient subsequently imposes an analog FT of these decaying enveloping z functions, this leads to the emergence of imaginary spectral components. As in the case of traditional 2D NMR a resolution to this problem could arise from combining a given z -decaying set with its mirror-image addition, so that when both of them are added together or combined in some other suitable fashion, the original even character of the z envelop is restored and the imaginary components arising upon the FT vanish [13]. To consider such possibility we use again Eq. (2) as our starting point but take now into account the fact that, given the dependence of a majority of homo- and hetero-nuclear mixing sequences on the phase of the rf, the spatial encoding in most 2D NMR experiments will show up as an amplitude rather than a phase modulation. When considering this one may, without loss of generality, rewrite the indirect-domain signals as

$$S(k) = \frac{M_0}{N_1} \sum_{j=0}^{N_1-1} \cos[C\Omega_1(z_j - z_{N_1})] \times \exp\left\{\frac{-C(z_j - z_{N_1})}{T_2}\right\} \exp\{ikz_j\}. \quad (10)$$

This equation suggests a simple route to acquiring complementary data sets possessing mirror-imaged z decaying functions, which results from combining the original $[+G_a/-G_a]_{N_2}$ gradient echo acquisition with a conjugate $[-G_a/+G_a]_{N_2}$ echo train. When viewed as a function of the z axis, the reversal imparted in this manner on the sign of k amounts to reversing the sense of the spatial encoding imposed by the internal Ω_1 coupling, while leaving unchanged the decay imposed by relaxation processes. Adding an “encoded” $S_e(k, t_2)$ data set to an “anti-encoded” $S_{ae}(-k, t_2) = S_e(k, t_2)^*$ one, thus provides a mean to eliminate the imaginary components introduced by relaxation during the course of the indirect evolution, and with it the phase-twist artifacts that may otherwise appear in the 2D spectrum. Fig. 5 illustrates an experimental investigation of these features and procedures, using a 2D ^1H TOCSY NMR experiment on a D_2O solution of L-cysteine hydrochloride as example. The improvements in the peak shapes that result from combining the encoded and anti-encoded sets are evident, both when comparing the spectra in phase-sensitive as well as in magnitude modes. Notice that there is a connection between this choosing of the k -variable sign for the sake of decoding one of two possible z spatial windings, and the usual 2D NMR selection of complementary echo/anti-echo coherence transfer pathways: both of these alternatives are then capable of removing dispersive components by symmetrizing relaxation effects along their respective indirect-domain encoding domains— z and t_1 , respectively.

¹ Similar mixed-phased line shape effects are expected when considering spectra acquired in ultrafast NMR experiments involving three or more dimensions [11].

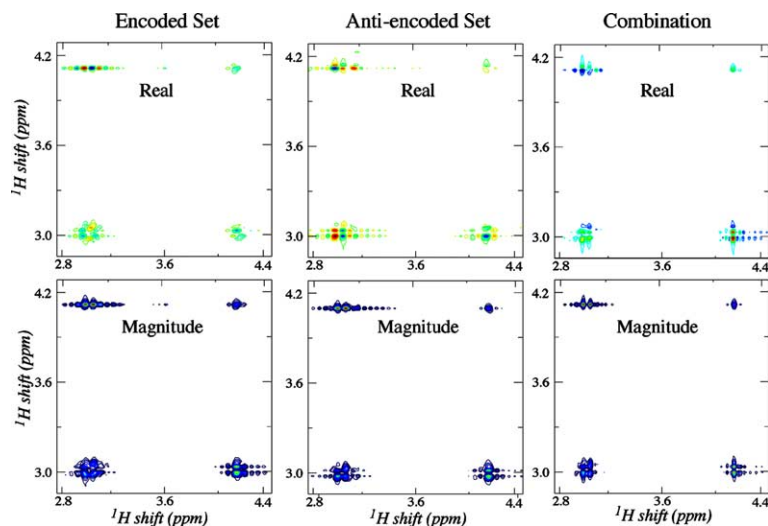


Fig. 5. Strategy capable of eliminating mixed-phase line shape components arising from spin relaxation, as exemplified with a series of ultrafast ^1H TOCSY NMR experiments collected on a cysteine/ D_2O solution. “Encoded” k/v_1 data demodulated with the conventional $[+G_a/-G_a]_{N_2}$ square-wave acquisition train (left-hand data sets) are combined with “anti-encoded” mirror image data retrieved using $[-G_a/+G_a]_{N_2}$ acquisition gradients (center panel), to afford a relaxation-symmetrized data set whose $t_2 = 0$ slice is ideally free from dispersive contributions. Data shown were collected with a 2 s HDO presaturation pulse using $N_1 = 50$ rectangular excitation pulses, $250\ \mu\text{s}$ long each and spread 4 kHz apart. Other parameters include $\gamma_e G_e = 120\ \text{kHz/cm}$, $\gamma_a G_a = 60\ \text{kHz/cm}$, $T_a = 395\ \mu\text{s}$, $N_2 = 80$.

The line shape improvements introduced by the encoding/anti-encoding procedure just described were achieved at the expense of incrementing the number of acquired scans to two—not a negligible increase when dealing with ultrafast NMR experiments. It is still possible to retain the single-scan character of these 2D acquisitions while collecting all data that are needed for eliminating the dispersive line shape components, if experimental parameters are set in a manner such that k -echoes generated by both encoded and anti-encoded windings can be simultaneously accommodated within a single T_a decoding time. In order to implement such “full-decoding” detection mode it is convenient to tune the acquisition parameters so that (i) the full k excursion taking over the course of each T_a suffices to cover twice the desired range of SW_1 frequencies, (ii) the echoes arising from encoded and anti-encoded coherences do not overlap, and (iii) the edges of the two decoding processes fall at approximately the center of the k -excursion, i.e., that $k \approx 0$ falls at ca. $T_a/2$. At least three independent variables are at the experimentalist’s disposal to simultaneously achieve these various conditions: the difference $\Delta\phi$ between the phases of the consecutive pulses involved in the initial excitation train (or equivalently, the overall carrier offset ω_o around which the train of the excitation pulses is built), the application of a pre-mixing gradient pulse capable of adding onto the Ω_1 -induced spiral of magnetizations an additional encoding

$$k_{\text{pre}} = \gamma_e \int_0^{\tau_{\text{pre}}} G_{\text{pre}}(t') dt',$$

and the application of a post-mixing gradient pulse capable of shifting the peaks’ position along the k/v_1 domain by an additional constant

$$k_{\text{post}} = \gamma_a \int_0^{\tau_{\text{post}}} G_{\text{post}}(t') dt'.$$

The first two of these variables can enable a total separation of encoded and anti-encoded echo peaks by changing the z encoding from that described in the amplitude-modulated term of Eq. (10) into $\cos[(C\Omega_1 + \Delta\phi + k_{\text{pre}})(z_j - z_{N_1})]$, while the latter enables peaks to be centered in the acquisition window by changing the final decoding term in Eq. (10) to $\exp(i(k + k_{\text{post}})z_j)$. Figs. 6 and 7 illustrates various features involved in this full-decoding strategy for retrieving purely-absorptive 2D NMR line shapes within a single scan, using a three-pulse 2D ^1H NOESY NMR experiment on an artificially-broadened 0.1% $\text{H}_2\text{O}/\text{D}_2\text{O}$ solution as example. Shown first in Fig. 6 is the realization of this single-scan acquisition of a pair of complementary 2D NMR spectra, identical in almost every respect except for their peaks being mirrored-image along the indirect domain about the $k = 0$ coordinate. These two sets can then be separated and subject to a treatment analogous to the one expounded previously for the case of independent encoded/anti-encoded acquisition. Fig. 7 focuses in further detail on this process, stressing the fact that the z -symmetrization and ensuing elimination of mixed-phase components that it has associated can actually be carried out in more than one fashion. Indeed one possibility is to simply subject the resulting data sets to minor phase adjustments and

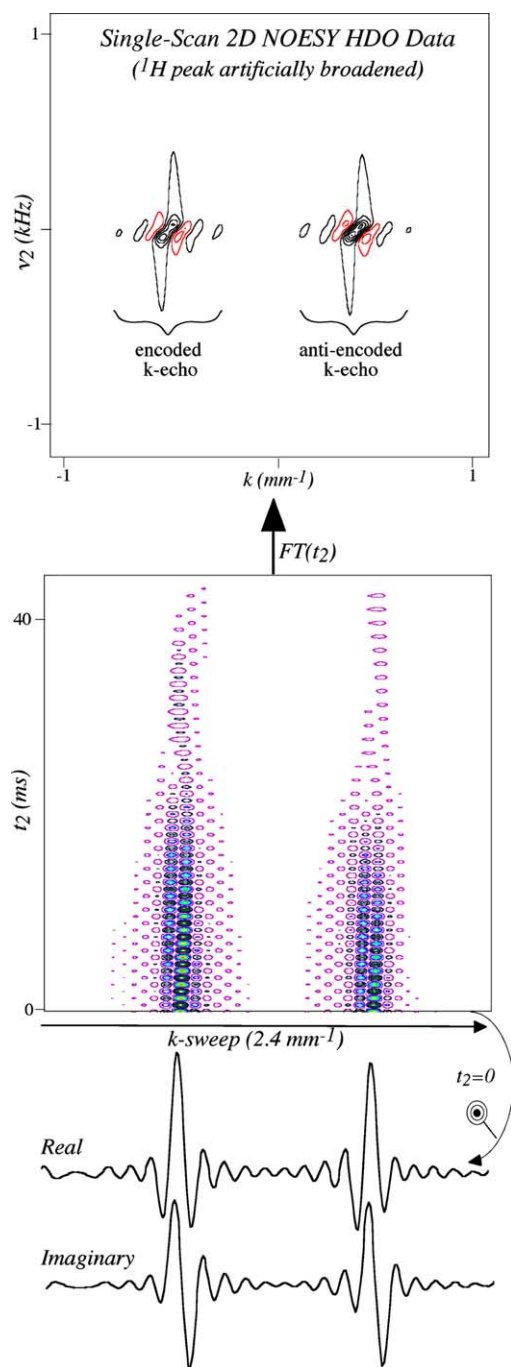


Fig. 6. Simultaneous acquisition of encoded and anti-encoded 2D NMR spectra within a single scan, illustrated with a model NOESY-type 2D experiment implemented on the proton resonance of an artificially broadened HDO sample. Experimental parameters ($N_1 = 36$ rectangular excitation pulses 10 kHz apart, $\gamma_e G_e = 205$ kHz/cm, $\gamma_a G_a = 150$ kHz/cm, $N_2 = 64$) were set so as to achieve a full-decoding of both echo and anti-echo transfer pathways, as evidenced by the mirror-imaged set in the center panel. Notice the dispersive component present in this case along the $t_2 = 0$ slice owing to spin relaxation during t_1 (bottom). FT of the data along t_2 (top) leads to 2D NMR spectra that are mirror-imaged along $k = 0$, whose peaks possess mixed-phase character (black/red contours imply positive/negative levels, respectively). For an interpretation of the references to color in this paper, please refer to its web version).

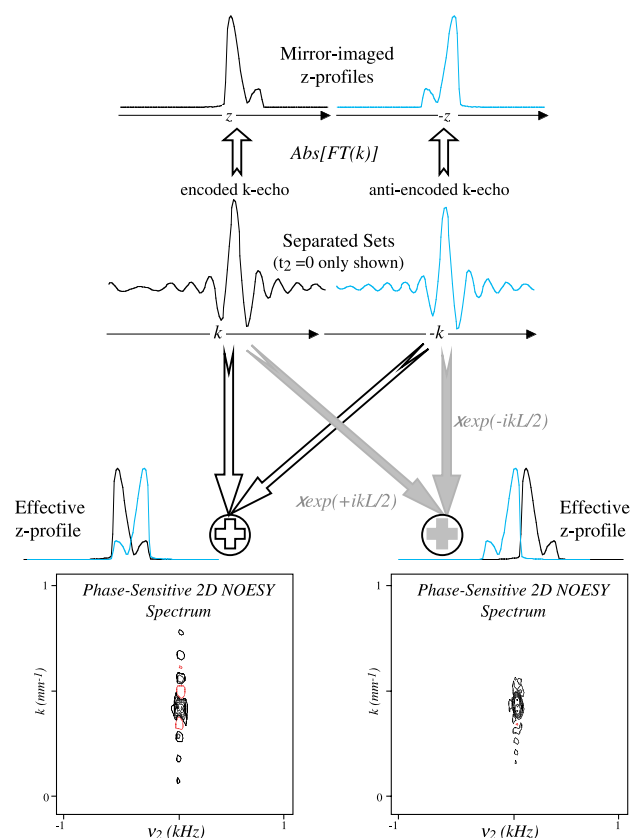


Fig. 7. Retrieval of dispersive-free 2D NMR line shapes from the full-decoding data set introduced in Fig. 6. In such processing encoded and anti-encoded 2D data are first separated (center panel, only $t_2 = 0$ slices shown for simplicity) leading to the equivalent of the independent encoded/anti-encoded data sets introduced in Fig. 5. The overall z -symmetry (equivalent to t_1 symmetry in conventional 2D NMR) can then be reinstated by directly adding the two sets (left-hand spectrum), or by performing a suitable first-order phase correction and only then combining the sets (right-hand spectrum). In either case dispersive components along the indirect domain are removed; in the second case an overall improvement is also retrieved in the 2D kernel shape, and fewer Sinc “wiggles” results.

subsequent addition, a procedure which solely leads to a cancellation of the dispersive components for $t_2 = 0$ (Fig. 7, left-hand 2D spectrum). A second possibility is to subject the two data sets prior to their recombination to sizable $\exp(\pm ikL/2)$ first-order phase corrections, which not only remove the dispersive components but also lead to a doubling in the effective length of the sample size and consequently to an additional resolution enhancement of the peaks. The ensuing line shape improvement is clearly visible in simulations or when dealing with a single well-defined peak (Fig. 7, right-hand spectrum). The improved phase-sensitive and magnitude line shapes illustrated in Fig. 5C were also obtained as a result of using such procedure based on sizable first-order phase corrections.

Before concluding this paragraph it is worth noting that although performed within a single scan, the dis-

persive-elimination approach illustrated in Figs. 6 and 7 exhibits two drawbacks when compared to the two-scan encoding/anti-encoding method in Fig. 5. One is a practical one, stemming from the need to fit twice the regular spectral window SW_1 within the same T_a scan time. All other parameters remaining equal this implies that either a sacrifice needs to be made on the ν_1 spectral resolution, or G_a gradients that are twice as strong will be needed over the course of the acquisition. This is similar to the demand made by TPPI for the doubling of the effective SW_1 window, a feature that can be rationalized when considering that full-decoding behaves as a spatial analog of the TPPI approach. A second, more fundamental limitation from this method stems from the fact that during its course, encoded and anti-encoded k -echoes corresponding to the same chemical site are not generated at strictly identical t_2 times. This complication, which does not apply to the two-scan procedure illustrated in Fig. 5, brings about additional phasing requirements which complicate the retrieval of dispersive-free line shapes. Certain alternatives to obtain dispersive-free spectra like the implementation of constant-time approaches, bypass such complications and are capable of affording purely absorptive line shapes while retaining the single-scan nature of the experiment. Additional strategies to retrieve purely-absorptive line shapes can also be conceived; considerations on these matters will be presented in further detail in a future publication.

3.3. Signal intensity considerations

Another issue to consider when exploring the applicability of ultrafast 2D NMR experiments is the signal intensity that will characterize this type of acquisitions. This paragraph is devoted to such analysis, using Eq. (5) as starting point. According to this expression the $S(k)$ echoes generated during the course of the ultrafast signal acquisition will, in the absence of relaxation or of any other dissipative/storage processes associated to the mixing sequence, be proportional to the full magnetization M_o generated by all spins throughout the sample. Not taken into account in such derivation, however, are the repetitive dephasing/rephasing processes that individual spin-packets themselves will undergo upon being acted by the various gradient-echo trains in the pulse sequence. As discussed in the Appendix of Ref. [7] such intra-slice dephasing/rephasing processes will leave all $\{A_j\}$ amplitudes equal but will transform them from constants to k -dependent functions. In the linear regime approximation such functions can be shown to depend on details of the excitation pulse—nutration rate $\gamma_e B_1^o$ and rf pulse shape $E(t)$ —as well as on the gradient $\gamma_e G_e$ defining spatial selectivity during the course of the excitation, according to

$$A_j(k) \approx \gamma_e B_1^o \frac{M_o}{L} \times \int_{-\infty}^{+\infty} E(t) \left[\int_{-\infty}^{+\infty} e^{-i(\gamma_e G_e T_p/2 - k - \gamma_e G_e t)\delta z} d(\delta z) \right] dt \quad (11a)$$

$$= \gamma_e B_1^o \frac{M_o}{L} \int_{-\infty}^{+\infty} E(t) \cdot \delta(\gamma_e G_e T_p/2 - k - \gamma_e G_e t) dt \quad (11b)$$

$$= \frac{\gamma_e B_1^o}{\gamma_e G_e} \frac{M_o}{L} E\left(\frac{T_p}{2} - \frac{k}{\gamma_e G_e}\right) \quad (11c)$$

At first glance, it is not evident from this expression where the $A_j = M_o/N_1$ dependence assumed above comes from. This origin can be best appreciated when considering an excitation that is executed via a train of $\pi/2$ square-shaped pulses, where the individual $E(t)$ functions are constant within each pulse time T_p and where the pulse excitation bandwidths can be approximated as $\Delta O \approx 1.5/T_p$. The T_p length for each individual pulse of the excitation train will then be tuned to

$$\gamma_e B_1^o \int_{-T_p/2}^{T_p/2} E(t) dt = \gamma_e B_1^o T_p E(0) = \pi/2,$$

since the number of excitation pulses N_1 that are used in this kind of experiments is usually optimized to match the ratio $\gamma_e G_e L/\Delta O$, this implies that Eq. (11c) can be rewritten for the case of square excitation pulses as $A_j^{\text{square}} \approx (M_o/6N_1)$. This M_o/N_1 dependence is as predicted in the arguments from the preceding paragraphs, while the additional 1/6 factor scaling the overall intensity arises from arguments related to the linear regime approximation, and as such its nature is not relevant.² When repeated for other pulse shapes similar calculations predict slightly bigger scaling factors ($\approx 1/5$ and $1/4$ for Gaussian- and Sinc-shaped pulses, respectively). Numerical simulations and experiments also confirm that minor differences in the maximum relative intensities result upon using different excitation pulse shapes.

An important prediction made by Eq. (11c) is that the peaks' profile along the indirect k/ν_1 domain, will appear proportional to the pulse shape $E(t)$ used to achieve the spins' excitation. A dilute 0.1% HDO sample was once again employed to experimentally test this dependence, by scanning the apparent offset of the single resonance that is then observed along k/ν_1 and measuring its amplitude for a variety of typical excitation pulse shapes. Fig. 8 illustrates the various intensity profiles observed along the indirect ν_1 dimension when

² Still, one could expect a scaling factor smaller than unity due to the fact that a square pulse will bring about a Sinc-like excitation profile of the spins, and hence a certain portion of the magnetization available in the slice will remain unused.

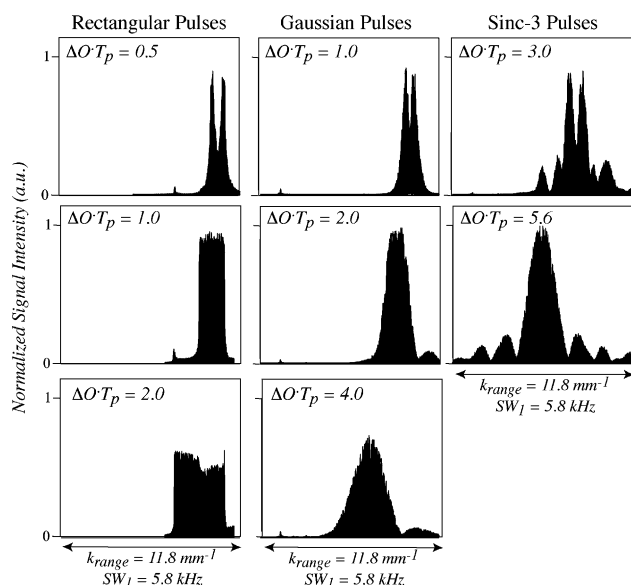


Fig. 8. Experimental illustration of the Rf excitation pulse enveloping effect, as manifested by the indirect-domain signal intensity (magnitude mode) arising from a 0.1% HDO sample as a function of its irradiation offset. In all cases a mixing-less pulse sequence was employed, and 160 frequency-offsetted experiments were repeated along the indicated range. Except for the pulses' shape all experimental parameters were common and involved $N_1 = 32$, $\gamma_e G_e = 98$ kHz/cm, $\gamma_a G_a = 38$ kHz/cm, $\Delta O = 10$ kHz frequency increments.

utilizing square, Gaussian and Sinc pulse shapes for the excitation. Also shown are the profile changes that were observed for each pulse shape upon varying the $\Delta O \cdot T_p$ product from a situation of no overlap between the excited slices (Fig. 8, bottom row), to one of severe overlap between these slices (top row). As all experiments were collected under identical conditions (including identical overall evolution times), it also becomes possible to compare the relative signal intensities afforded by these different excitation modes. First to notice from the center-row results, collected using offset increments ΔO leading to an immediate adjacency among the excited slices, are the different profiles exhibited by the peaks' intensities as a function of offset. These are square-like when using square excitation pulse, Gaussian-like for Gaussian pulses, and Sinc-like for lobed Sinc pulses. This is as predicted by Eq. (11c) and implies that, except when using square excitation pulses or otherwise correcting for the pulse shape employed, non-quantitative results will be extracted from ultrafast 2D NMR peak volumes. Also interesting to note are the stretchings and contractions exhibited by the spectral envelopes of the various columns, reflecting in turn the different pulse lengths T_p used in their respective excitations. The maximum signal intensity is always accomplished when the $\Delta O \cdot T_p$ product reaches the adjacency condition; ca. 1.5, 2.2, and 5 for square, Gaussian and 3-lobed Sinc pulses, respectively. On extending the pulse lengths beyond these adjacency conditions the overall signal in-

tensities begin to drop, reflecting the unexcited sample regions that are left out by this choice; still, the overall peaks' line widths remain constant. A reduction of the $\Delta O \cdot T_p$ product below the adjacency condition also leads to a mild drop in the signals' intensities, but is also accompanied by a distortion in the overall offset envelop and a broadening of the echo peaks. Numerical simulations validate very well all these experimentally observed changes; they also predict that for all kind of pulse shapes there is a fairly broad region of $\Delta O \cdot T_p$ values in the neighborhood of the adjacency condition ($\approx \pm 25\%$) over which no significant envelop distortions, peak broadenings or signal losses will occur.

The enveloping effects that the pulse shape $E(t)$ imparts on the region of the k/v_1 axis where echo peaks can be expected, also place a practical constraint on the spectral widths which can be scanned along the indirect domains of ultrafast 2D NMR experiments. Thus, in addition to the

$$SW_1 = \left| \Delta O \frac{\gamma_a G_a T_a}{2\gamma_e G_e T_p} \right|$$

expression derived in [6,7] as defining the v_1 spectral equivalent that is scanned by the acquisition variable k , Eq. (11c) implies that it is not worth spanning an extent of k values that exceeds by much $\gamma_e G_e T_p$. Assuming negligible gradient switching times then suggests setting $k_{\max} = \gamma_a G_a T_a = \gamma_e G_e T_p$, and leads to $SW_1^{\max} \approx (\Delta O/2)$. In practical applications we observe that non-idealities make the attainable indirect spectral widths slightly larger than this expectation (ca. by 10%). This $\Delta O/2$ value is sufficient for covering the required spectral widths in a majority of homonuclear ^1H NMR experiments and in certain heteronuclear correlations experiments where only a restricted range of ppm needs to be monitored (e.g., the ^{15}N amide region or the ^{13}C α -carbon region in protein NMR studies), yet place a limitation when attempting to cover a full range of heteronuclear chemical shifts. A brute-force solution to this problem could come from increasing the strength of the field gradients employed and thus enable an increase in the ΔO values used without compromising on the number of N_1 slices involved in the encoding; more elegant solutions involving different excitation modalities are also conceivable and will be discussed and illustrated elsewhere.

3.4. *S/N and the limit of detection of ultrafast 2D NMR*

The preceding paragraph demonstrates that in the absence of substantial mixing-period losses and under relaxation-free conditions, only a slight decrease in signal intensity will be incurred by the selective excitation and gradient echo protocols associated to the acquisition of ultrafast 2D NMR spectra. Still it is known that not signal intensity but S/N ratio is the dominant

parameter defining the sensitivity of a particular spectroscopy technique and with it the limit of detection (LOD) that can be spectroscopically analyzed; we devote this last paragraph to examining the minimal LODs that can nowadays be studied via single-scan 2D NMR.

As a first experimental test on how does the absolute signal intensity that is observed in ultrafast 2D NMR acquisitions compare with its single-scan 1D counterpart, the time-domain signal amplitude of a 0.1% HDO sample was measured on-resonance for the following sets of experiments: a single-pulse excitation followed by a free-evolution acquisition, an offset-incremented gradient-echo excitation followed by a free-evolution acquisition, and an offset-incremented gradient-echo excitation followed by acquisition in the presence of oscillating gradients. The first of these experiments amounts to a conventional one-scan ^1H NMR acquisition, the last one constitutes a full mixing-less ultrafast 2D NMR experiment, while the second one entails solely the excitation module of the single-scan 2D NMR experiment. Results arising from these tests are summarized in Table 1, and clearly show that the theoretical $1/4 - 1/6$ scaling factors predicted by the linear excitation arguments are in fact exaggerate; in accordance with what we have noted throughout extensive numerical simulations, experimental measurements show that little (if any) signal intensity is lost due to the selective excitation and/or gradient-echo acquisition conditions involved by ultrafast 2D NMR.

Given the similar NMR signal intensities observed in mixing-less single-scan 2D experiments vis-à-vis conventional single-scan 1D acquisitions, it follows that the main S/N losses that will arise in realistic ultrafast 2D NMR acquisitions will come from (i) the penalties in signal intensity associated to the amplitude modulation and other dissipative processes conventionally present in 2D sequences but not in 1D NMR experiments, and (ii) the increased noise that in the ultrafast NMR protocol will be present due to its need to rapidly sample two independent axes (k and t_2) instead of just the usual acquisition time t of conventional 1D NMR. The former penalty will of course depend on the experiment being considered, on the spins' relaxation rate, on the quality

of spin decoupling during t_1 , etc.; for the sake of proceeding with a semi-quantitative discussion we will consider it to be $\approx 1/4$ —half of these losses coming from the fact that only one of the encoded pathways is detected, and the remaining half attributed to all other potential decays and non-idealities. As for the noise penalty its upper limit can be theoretically estimated as $\sqrt{2\gamma_a G_a L T_a}$, the square root of the increase in filter width which will have to be made in order to accommodate a simultaneous sampling along the two dimensions. Assuming typical conditions $\text{SW}_2 = (2T_a)^{-1} \approx 5$ kHz and $\gamma_a G_a L \approx 200$ kHz leads to an estimated noise increase of ca. 6. This noise factor was once again experimentally tested by carrying out a series of measurements on the dilute HDO sample as a function of filter width (Table 1), and found remarkably correct.

In view of these additional losses, what could one thus quote as a contemporary LOD value for a single-scan 2D NMR experiment? An estimate of this can be based on the S/N specification available for the NMR instrument used throughout the present study: ≈ 1750 for a single ^1H NMR scan acquired on a 0.1% ethylbenzene solution inside a 5 mm NMR tube at 18.8 T. On dividing this figure by the combined factors derived in the preceding paragraph predicts a S/N of ca. 8 for a single-scan 2D ^1H correlation spectrum acquired on a 1 mM sample. Although such S/N is somewhat marginal and numerous scaling factors in the preceding derivations could be considered ill-defined, these arguments would suggest contemporary LODs for single-scan 2D NMR in the 1–10 mM range. We consequently set out to explore the results that could be obtained in various 2D ultrafast experiments when investigating analytes within this concentration range. Fig. 9 for instance illustrates 2D HSQC results obtained on what was perhaps the most challenging of the systems that were analyzed in these tests, consisting of a 10 mM ^{15}N -labeled ubiquitin solution in 93%/7% $\text{H}_2\text{O}/\text{D}_2\text{O}$ incorporating a 50 mM potassium phosphate buffer (and sodium azide for preservation). Presumably due to the high solute and salt concentrations employed in the preparation of this solution a doubling resulted in the length of the minimum ^1H $\pi/2$ pulse achievable at maximum transmitter

Table 1
Relative signal and noise levels measured for a variety of single-scan experiment^a

Experiment	Signal level	Noise level
Singles-Pulse ^b ; Filter Width = 13 kHz ^c	1.0	2.3×10^{-4}
Singles-Pulse ^b ; Filter Width = 125 kHz ^d	1.00	9.2×10^{-4}
Singles-Pulse ^b ; Filter Width = 625 kHz ^d	1.0	1.5×10^{-3}
Selective excitation ^e ; Filter Width = 125 kHz ^d	0.83	6.4×10^{-4}
Ultrafast 2D NMR ^e ; Filter Width = 125 kHz ^d	0.83	–

^a Measured in the time-domain on a 0.1% $\text{H}_2\text{O}/\text{D}_2\text{O}$ solution at 18.8 T.

^b Using a $\pi/2$ excitation 11 μs long, with the signal intensity defined by the initial and final portions of the FID.

^c As achieved by digital filtering.

^d Analog mode filtration.

^e Using $N_1 = 56$ selective excitation pulses with $\Delta O = 6$ kHz and $\gamma_e G_e = 180$ kHz/cm.

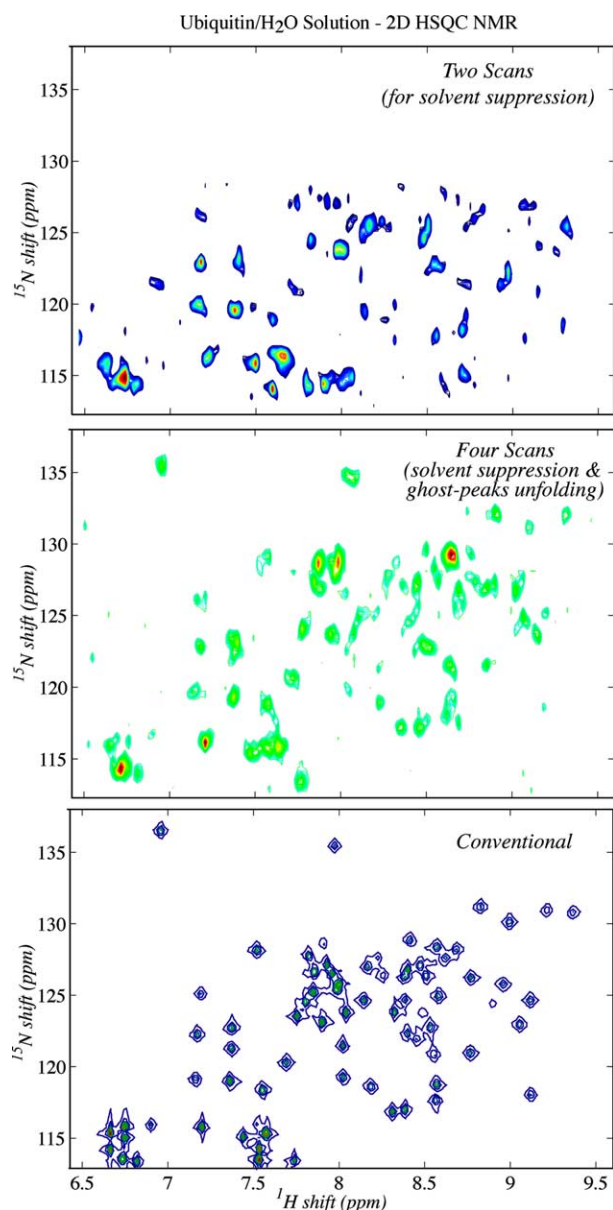


Fig. 9. Experimental verification of ultrafast's NMR capability to retrieve 2D NMR spectra from protein samples in a reduced period of time, using a ^{15}N - ^1H HSQC NMR experiment collected in a 10 mM Ubiquitin/water sample as example. The ultrafast acquisitions (top and center) involved $N_1 = 16$, $N_2 = 64$, $\Delta O = 2.6$ kHz, $365 \mu\text{s}$ long square excitation pulses, $\gamma_e G_e = 22$ kHz/cm, $\gamma_a G_a = 108$ kHz/cm, $2 \mu\text{s}$ physical dwell time; data were zero-filled to 128×128 ($k/v_1, t_2$) matrices prior to 1D FT. The conventional experiment (bottom) was the result of a 256×1024 (t_1, t_2) point acquisition involving an 8-scan phase cycling per t_1 point and 2 dummy scans; it took 51 min total acquisition time. The selective excitation ^{15}N pulse and the receiver demodulation were phase-cycled 180° in the two-scan experiment for the sake of removing residual ^1H signals not suppressed by the final Watergate gradients [14]; the four-scan experiment involved both this phase cycle scheme as well as a complementary time/space-shifted acquisition for the sake of unraveling folded "ghost"-peaks [8].

power (from 11 to $22 \mu\text{s}$), hinting to a corresponding 1/2 loss factor scaling the signals' intensities. Deficiencies were also found in the performance of the Watergate

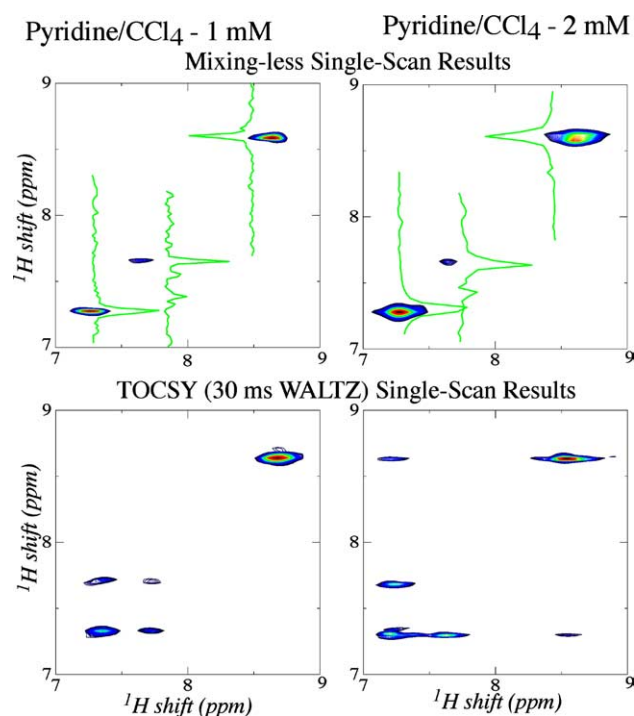


Fig. 10. Limit-of-detection tests of ultrafast 2D NMR, as revealed by mixing-less (top) and TOCSY (bottom) single-scan ^1H acquisitions on dilute solutions of pyridine in freshly distilled CCl_4 at 18.8 T. All experiments involved $N_1 = 56$, $N_2 = 64$, $\gamma_e G_e = 216$ kHz/cm, $\gamma_a G_a = 108$ kHz/cm, $142 \mu\text{s}$ long square excitation pulses at $\Delta O = 7$ kHz frequency increments, an analog filtration of 125 kHz, zero filling to 128×128 data sets and magnitude calculation. Shown for clarity are the profiles arising in the mixing-less sequences for the three inequivalent sites in the molecule.

suppression sequence, leading to intense residual water artifacts even when employing G_x and/or G_y gradients for its operation. As a result of all these artifacts³ 2D ^{15}N - ^1H HSQC data were collected in two scans rather than in one, incorporating identical parameters except for a reversal in the phase of the selective ^{15}N excitation pulse and of the signal receiver. This led to a good suppression of the residual water signal and to the spectral set shown in Fig. 9, top. The S/N characterizing such spectrum is acceptable, but its analysis becomes complicated by the presence of folded "ghost-peaks" within the limited ^{15}N ν_1 axis. The origin of such peaks has been described elsewhere, as were methods for identifying and eventually separating folded ghost-peaks with the aid of a complementary 2D NMR acquisition [8]. Such complementary-scan approach coupled to the phase cycling solvent-suppression procedure lead to a total acquisition of four scans; the center panel in Fig. 9 illustrates ^{15}N - ^1H HSQC results obtained on processing the data arising from these four single-scan 2D acqui-

³ Which could in turn well be a reflection of our limited experience in the area of biomolecular NMR rather than limitations in the hardware or in the pulse sequence design.

sitions. The spectrum that is observed in this case, where ghost-peaks have now been unfolded, is comparable to the regular 2D NMR trace that can be recorded for the compound (Fig. 9, bottom) and enables the assignment of nearly 80% of residues in this labeled polypeptide.

The good S/N observed in the multi-scan experiments presented in Fig. 9 suggests that, were it not for the solvent suppression or ghost-peak complications, single-scan 2D NMR experiments could be collected from solutions whose concentrations are under 10 mM. To test this hypothesis additional samples consisting of 1 and 2 mM solutions of pyridine in freshly distilled background-less CCl_4 were prepared, and single-scan 2D ^1H NMR spectra were recorded both in the absence of mixing and on using WALTZ as an isotropic mixing sequence. Fig. 10 illustrates results obtained in such phase- and amplitude-modulated ultrafast experiments, and shows that the 1–2 mM LOD estimated by this analysis is indeed correct.

4. Conclusions

The main objective of the present study was to summarize certain important aspects of ultrafast 2D NMR, particularly issues related to the peak shapes and profiles that can be expected on using this methodology, the achievement of purely absorptive line shapes, and the kind of analyte concentrations that can nowadays be assayed with this method. To do so we used as starting point simple spin-packet arguments introduced in our previous presentations, and relied on them to derive a number of different features. We consider that some of the new vistas that were thus derived, for instance the effects of relaxation on the observed line shapes, are of a fundamental nature and unlikely to change regardless of the actual pulse sequence used in the 2D acquisition. Still others, including the different approaches which could be used to shape the spins' excitation, to achieve purely absorptive 2D peaks, or the limits of detection of single-scan 2D acquisitions, are likely to be eventually superseded. A topic we feel particularly worth of attention is that related to the single-scan acquisition of purely-absorptive 2D line shapes, as although all the alternatives that were hereby discussed work in principle, they are subject to serious limitations with our available hardware. Regardless of these and other

technical considerations, general conclusions that follow from our arguments include (i) that mixed phase line shapes will arise when $2N_1 T_p \geq T_2$, a situation that is instrumentally unlikely to be fulfilled within the near future for small molecules but liable to happen when dealing with medium-sized proteins (or when dealing with broad lines due to poor shimming or inefficient decoupling); and (ii) that a factor of ca. 20 will degrade S/N when comparing single-scan 2D NMR vs conventional single-scan 1D acquisitions, thus currently limiting the per-scan LOD of the technique to analytes in the mM concentration.

Acknowledgments

This work was supported by the Philip M. Klutznick Fund for Research, by the Minerva Foundation (Munich, FRG), as well as by a grant from the Henry Gutwirth Fund for the Promotion of Research. A.L. is also grateful to the Feinberg Graduate School of The Weizmann Institute for an Anne Stone fellowship.

References

- [1] K. Wüthrich, *NMR of Proteins and Nucleic Acids*, Wiley, New York, 1986.
- [2] R.R. Ernst, G. Bodenhausen, A. Wokaun, *Principles of Nuclear Magnetic Resonance in One and Two Dimensions*, Clarendon, Oxford, 1987.
- [3] D.M. Grant, R.K. Harris (Eds.), *Encyclopedia of NMR*, Wiley, Chichester, 1996.
- [4] J. Jeener, in: *Ampere International Summer School II*, Basko Polje, Yugoslavia (1971).
- [5] W.P. Aue, E. Bartholdi, R.R. Ernst, *J. Chem. Phys.* 64 (1976) 2229.
- [6] L. Frydman, T. Scherf, A. Lupulescu, *Proc. Natl. Acad. Sci. USA* 99 (2002) 15858.
- [7] L. Frydman, T. Scherf, A. Lupulescu, *J. Am. Chem. Soc.* 125 (2003) 9204.
- [8] Y. Shrot, L. Frydman, *J. Magn. Reson.* 164 (2003) 351.
- [9] D.J. States, R.A. Haberkorn, D.J. Ruben, *J. Magn. Reson.* 48 (1982) 286.
- [10] D. Marion, K. Wüthrich, *Biochem. Biophys. Res. Commun.* 113 (1983) 967.
- [11] Y. Shrot, L. Frydman, *J. Am. Chem. Soc.* 125 (2003) 9204.
- [12] M. Levitt, *Spin Dynamics*, Wiley, New York, 2001.
- [13] E.O. Brigham, *The Fast Fourier Transform*, Prentice Hall, Englewood Cliffs, 1974.
- [14] M. Piotto, V. Saudek, V. Sklenar, *J. Biomol. NMR* 2 (1992) 661.